Polymer 51 (2010) 2337–2344

Contents lists available at ScienceDirect

Polymer

journal homepage: www.elsevier.com/locate/polymer

# Interplay of kinetics and interfacial interactions in breath figure templating – A phenomenological interpretation

Eva Servoli*, Giuseppe A. Ruffo, Claudio Migliaresi

*BIOtech – Department of Materials Engineering and Industrial Technologies, INSTM Research Unit – University of Trento, via delle Regole 101, Mattarello, 38100 Trento, Italy*

ARTICLE INFO

*Article history:*
Received 14 July 2009
Received in revised form
22 February 2010
Accepted 23 March 2010
Available online 31 March 2010

*Keywords:*
Breath figures
PDLLA
Porous structures

ABSTRACT

Breath Figure BF templating is an attractive technique for the production of polymer films with controlled porosity: upon the exposure to a moist airflow, monodisperse water droplets condense on the surface of evaporating polymer solution into ordered arrays, acting as a template for the final film structure.

This work has been focused on polylactic acid (PDLLA), a biocompatible biodegradable polymer, and aims to provide a phenomenological interpretation of BF process based on the role of kinetics and the influence of interfacial tension. The effects of physical and chemical properties of solvents have been evaluated; the contribution of kinetics has been assessed by modifying the rate of film hardening from seconds to minutes, via different experimental set-up. Our experimental observations indicated that the interplay of kinetics and interfacial tension defines the structure of BF films: interfacial forces govern the physical interactions among water, solvent and polymer, but the dynamics of the process and thus the final pore structure is regulated by kinetics.



## 1. Introduction

Polymer films with controlled porosity are attractive for a variety of applications, from photonics to biomedical devices [1]. Many different techniques are currently employed in the production of porous substrates, but self-organization of matter is arising as the most convenient approach. Among them, Breath Figure templating is regarded as a simple and cost effective technology since François and coworkers first observed the phenomenon [2].

Breath Figures are patterns originated by water drops that condense as isolated objects from moist air upon contacting a cold solid or liquid surface. When the pattern is formed on a solution casting film, the droplets print pores on the surface. This physical phenomenon has been studied all across the XX century [3–6] and is currently exploited for BF templating as it follows: (i) polymers are dissolved in solvents with high vapour pressure and low miscibility with water; (ii) the solution is allowed to dry in a humid environment, generally under flow conditions, in order to induce water condensation and nucleation of water droplets at the air/liquid interface; (iii) during the first stages of solvent evaporation water droplets slowly grow by uptake of moisture from the surrounding water vapour, without merging; (iv) after a few seconds droplets start to experience coalescence and their radius R increases with time according to $R \sim t^{1/3}$ [7]; (v) water droplets self-organize into regular patterns while growing, thus creating a template for the subsequent arrangement of polymer chains: as film hardening occurs and the evaporation of water is completed, a regular porous structure is obtained.

Pore size can range from a few hundreds of nanometers to several micrometers depending on the experimental conditions, as relative humidity, the rate of moist airflow, surface temperature, polymer concentration, polymer architecture, interfacial tension between solvent and water [8–10]. The same parameters are also believed to regulate the arrangement of water drops into honeycomb patterns, preventing or reducing coalescence: soon upon condensation, water drops have high mobility on the surface and attractive interfacial forces induce the aggregation of few drops into small ordered areas; later on, a force proportional to the sixth power of area radii attracts other ordered islands, thus extending the regular pattern [11]. Although the mechanism has not fully clarified, many experimental results indicate that airflow and thermocapillary flow drive the hexagonal packing of water drops: solvent evaporative-cooling causes a temperature gradient within the solution and a subsequent surface tension gradient is produced, with colder areas corresponding to regions at higher surface tension. At this point Marangoni convection produces a thermocapillary flow that directs the solution with water drops to colder areas in order to minimize surface energy, until the surface is completely covered by water drops [8,12]. As long as a temperature gradient is maintained, thermocapillary convection also prevents

* Corresponding author. Tel.: +39 0461883645; fax: +39 0461883091.
*E-mail address:* servolie@ing.unitn.it (E. Servoli).

0032-3861/$ – see front matter © 2010 Elsevier Ltd. All rights reserved.
doi:10.1016/j.polymer.2010.03.039

water drops from coalescence, inducing convective motion inside the drops and between them, where the presence of a lubricating air film has been demonstrated [13,14]. Alternatively, it has been suggested that non-coalescence is related to solvent vapour, which creates a separating layer between droplets [12].

Along with superficial patterns, multilayer structures with a regular arrangement of pores can be obtained via BF templating. However, despite the growing interest for the phenomenon itself and its technological implications, controversial models have been proposed to explain the formation of monolayer vs multilayer arrays: some reports relate the presence of pore multilayer to solvent density [12,15], others attribute pore stacking to interfacial tension [16,17]. This point will be discussed thoroughly in the subsequent sections.

In pioneering works only star polystyrene SPS and rod-coil block PS were believed to generate BF templating [2,7,18,19], nowadays a variety of polymers are currently employed, as reported in the reviews by Bunz [1] and Stenzel [10]: linear conjugated polymers, polyimides, light emitting polymers, liquid-crystalline polymers, organometallic polymers and degradable polymers. More recently, BF templating on biocompatible, biodegradable polymers has become very attractive for many biomedical applications, from tissue engineering to drug delivery [20–22].

The present work is intended as a phenomenological discussion about the mechanisms of BF templating on polylactic acid PDLLA, a biocompatible aliphatic polyester that is particularly attractive for its biodegradability. We report the formation of a variety of porous structures via BF templating on PDLLA solutions, by varying polymer concentration, solvent type, and experimental set-up; then the BF phenomenology on PDLLA has been related to processing conditions, in order to investigate the role of physical and chemical interactions, together with kinetics, in regulating the process.

## 2. Experimental

Linear Poly(D,L)Lactic Acid (PDLLA) Resomer R207 (MW = 200 kDa) was purchased from Boeringher Ingelheim (Germany). PDLLA was dissolved at room temperature in Chloroform (CHL) and Ethyl Acetate (EA) at 3%, 6%, 11% w/v concentration and used within 18 h to produce porous PDLLA films.

Porous films were obtained via BFs templating according to two different experimental set-up, in which the timescale of film hardening could be varied from seconds (spin coating system) to minutes (humid flow system).

The former set of samples was produced by casting the polymer solution under controlled humid flow (Fig. 1A): 600 μl of PDLLA solution were spread on glass slides and placed in a cylindrical chamber (3 cm diameter, 18 cm length), connected at one end to an air bubbler. Blowing compressed air into distilled water at room temperature generated moist air; the other end of the casting chamber was let open. Complete solvent evaporation required up to 15 min; the typical sample thickness was within 40 μm. Flow rate was adjusted between 0.8 and 1.4 L $min^{-1}$ according to polymer concentration, in order to avoid waving effects on the film surface and favor the regular arrangement of water droplets during water condensation.

The formation of BF patterns on PDLLA-CHL 6% (w/v) and PDLLA-EA 11% (w/v) has been observed in real time by optical microscopy (Axiotech, Zeiss) and videos have been recorded via a microscopy camera (Infinity, Lumenera); for this purpose the cylindrical chamber has been substituted with parallel-plate chamber in order to improve focusing. Average drop radius has been measured on individual video frames via the free software Gwyddion and plotted versus time; curve fitting has been carried out via Origin - Advanced fitting tool.

The second set of PDLLA films was produced via spin coating (Spin150 – SPS-Europe) under controlled humidity, generated by heating at different temperature a water bath inside the spin chamber (Fig. 1B); relative humidity RH of (78 ± 3)% or (87 ± 3)% were used for this study. Experiments were carried out as follows:

(i) 100 μl of polymer solution were loaded on a square cover glass (25 × 25 mm) while rotating at 6000 rpm; after few seconds the spin rate was reduced to 1000 rpm;
(ii) 300 μl of polymer solution were dropped on a square cover glass (25 × 25 mm) and spin coated at 4000 rpm for few seconds before reducing the spin rate to 1000 rpm.

Total spin time of 30 s was required for complete solvent evaporation; typical sample thickness was less than 5 μm.

All glass substrates were used as received.

Assuming that fast film hardening can freeze BF templating in its early stage, the analysis of porous films obtained on different timescales can thus indirectly describe subsequent steps of the process itself.

Film structure was characterized by light microscopy (Zeiss Axiotech 100 Hal) and Scanning Electron Microscopy (SEM), both in High Vacuum (Cambridge Stereoscan 200) and in Low Vacuum mode (Philips TMP ESEM), operating between 10 kV and 16 kV accelerating voltage.

Cross sections of the porous films were obtained by cryofracture in liquid nitrogen and analyzed by SEM as previously explained. All samples were gold sputtered before SEM analysis.

The image analysis software ImageJ was used to measure the average pore size of each sample and to calculate two-dimensional Fast Fourier Transform (2D-FFT) in order to characterize surface structures and identify the presence of regular patterns [23].

## 3. Results and discussion

Among organic solvents, Chloroform and Ethyl Acetate were selected for this study because of their volatility and good solubility for PDLLA; moreover, the differences of their physical and chemical

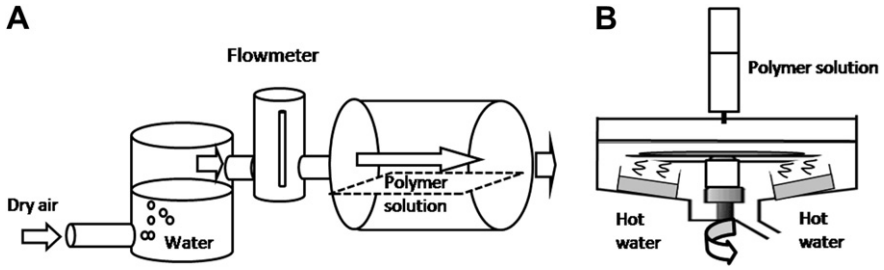


**Fig. 1.** Experimental set-up for the production of BF films: humid flow system (A) and spin casting approach. (B) In A compressed air is bubbled into water to generate moist air, the airflow is controlled by a flowmeter and inlet into the glass chamber, where polymer solutions are allowed to dry; in B polymer solutions are injected into the spin coater chamber, where a water bath ensures the desired values of relative humidity.

**Table 1**
Some relevant physical and chemical properties of solvents used in this study [24,25].

| Solvent | Surface tension | Interfacial tension with $H_2O$ | Density | Solubility in $H_2O$ | Vapour Pressure (@20 °C) | Enthalpy of Vaporization (@25 °C) |
|---|---|---|---|---|---|---|
| CHL | 27.5 mN $m^{-1}$ | 28.3 mN $m^{-1}$ | 1.48 g $cm^{-3}$ | 0.8 g/100 ml | 21.1 kPa | 31.68 kJ $mol^{-1}$ |
| EA | 23.9 mN $m^{-1}$ | 25.9 mN $m^{-1}$ | 0.89 g $cm^{-3}$ | 8.3 g/100 ml | 12.4 kPa | 35.66 kJ $mol^{-1}$ |

properties (Table 1) can give new insights into the contribution of solvent type to the entire process. CHL is a customary solvent for BF templating while EA is quite unusual for this application, possibly because of its higher solubility in water; however the low toxicity of EA makes this solvent an attractive choice.

### 3.1. Structure of BF films via humid flow system

Porous films with different structures were obtained in the humid flow chamber (Fig. 1A) by varying the solvent type and concentration.

The flow rate F was adjusted according to polymer concentration in order to optimize the regularity of the pore patterns and, under certain conditions, to control pore size (Fig. 2).

When PDLLA was dissolved in CHL, either multilayer pore structures or single layers of pores were produced depending on polymer concentration: 6% w/v solution created tridimensional porosity with at least three porous layers stacked up, where pore size increased from the bottom to the upper surface; conversely pore monolayer was produced by 11% solution. Irrespective of concentration, pores of films obtained in the humid flow system were interconnected, even if a reduced degree of interconnection was observed with higher polymer concentration.

Pore dimension was affected by the flow rate F, with larger pores produced by lower F values: the apparent diameter (i.e., pore lateral dimension measured on the film surface) was $d$=(11.1 ± 2.8) μm for $F$ = 0.8 L $min^{-1}$ while it was reduced to $d$=(5.1 ± 0.7) μm for $F$ = 1.2 L $min^{-1}$. Polymer concentration had no significant effects on pore size when PDLLA was dissolved in CHL and spherical-like pores with a typical aspect ratio $R$ = 0.8 were observed.

PDLLA-EA solutions produced a single layer of interconnected pores. Films obtained under flow rate $F$ = 1.2 L $min^{-1}$ with 6% w/v solution exhibited columnar pores with spherical basis of diameter $d$=(7.2 ± 1.6) μm and lateral walls of (15.7 ± 0.8) μm (aspect ratio $R$ = 0.5); interconnections were generally observed at the junction between pore walls and pore basis. Higher solubility of water in EA, with respect to other solvents commonly employed for BF templating, might be responsible for columnar pores.

In contrast to PDLLA-CHL system, PDLLA-EA produced smaller pores of $d$=(5.5 ± 0.3) μm by increasing polymer concentration to 11% w/v; pores exhibited a square-like shape ($R$ = 0.9) and lower degree of interconnection.

Although honeycomb structures could not be obtained by these experimental setups, 2D-FTT analysis of pore patterns [23] revealed that the higher level of order and regularity was achieved by dissolving PDLLA in chloroform (Fig. 3). The power spectrum of PDLLA-CHL films showed a six-fold modulation superimposed to a ring of weaker intensity, which indicates the presence of a characteristic interpore distance with preferred hexagonal order. PDLLA-EA produced a sharp ring, suggesting a random distribution of monodispersed pores.

### 3.2. Structure of BF films via spin casting procedure

In the spin casting procedure, PDLLA films were made under controlled humidity, by adjusting the spin rate to polymer

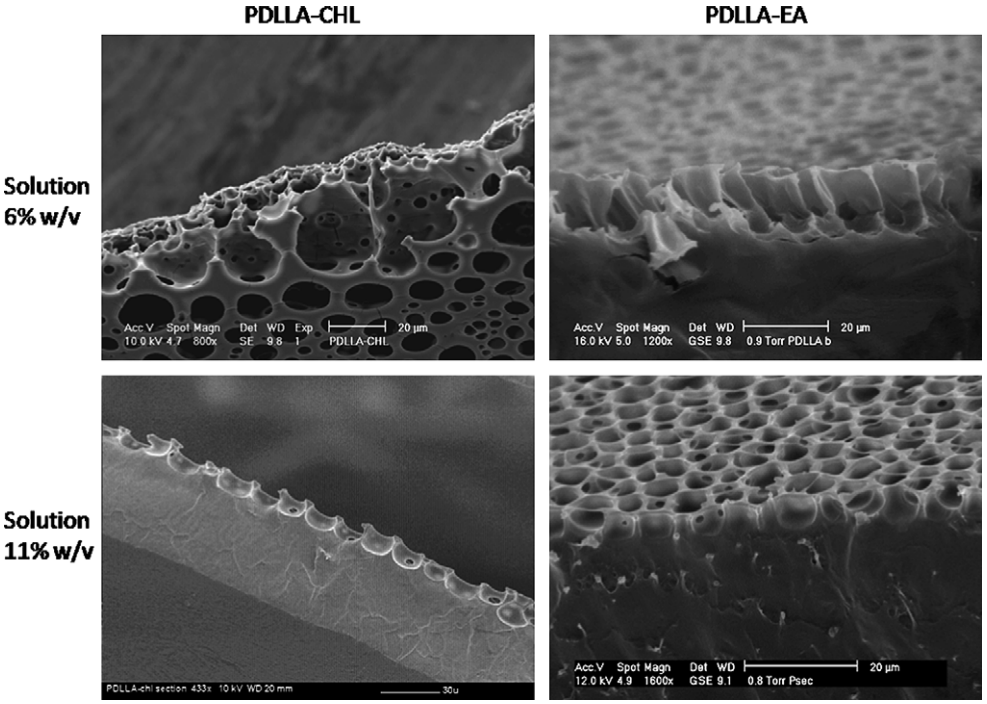


**Fig. 2.** Cross sections of BF films produced in the humid flow chamber. The effects of solvent type (columns) and polymer concentration (rows) on pore structure have been evaluated by SEM analysis.

concentration (Fig. 1B). Humidity values were varied in order to optimize the regular arrangement of water droplets and the subsequent regularity of porous films (Fig. 4).

BFs films with PDLLA solution 6% w/v in CHL were characterized by a single layer of individual pores, with tunable size according to the volume of solution loaded in the spin coater: 100 μl of solution produced pores of diameter (2.0 ± 0.3) μm and depth (1.0 ± 0.1) μm (aspect ratio $R = 2$), while 300 μl gave diameter of (2.2 ± 0.4) μm and depth of (1.7 ± 0.2) μm (aspect ratio $R = 1.3$).

When PDLLA was dissolved in EA (6% w/v), the volume of polymer solution had a different effect on the process: films with a single layer of pores were obtained from 100 μl, while two layers were stacked up after loading 300 μl. In the latter case, two layers of pores with constant diameter (3.7 ± 0.8) μm were piled up and interconnections were generally observed in-plane rather than out-of-plane; the bottom layer was (1.2 ± 0.1) μm depth, the top layer (1.5 ± 0.1) μm.

The value of relative humidity affected single layer films mostly: individual pores of depth (1.1 ± 0.2) μm were obtained at 78% RH, while deeper interconnected pores of depth (3.1 ± 0.1) μm were produced at 87% RH. Pore diameter was measured as (2.5 ± 0.4) μm in both cases, meaning that the aspect ratio of pores can be modified by changing the humidity parameters in the spin chamber: pore aspect ratio could be varied from $R = 2.3$ for 78% RH to $R = 0.8$ for 87% RH. In addition, lower humidity favored the formation of individual pores while interconnected pores were typically observed at higher RH values.

The 2D-FFT analysis of surface patterns (Fig. 3) showed an inverse trend of spin coated films with respect to the humid flow system: the power spectrum of PDLLA-EA exhibited diffuse spots in preferred directions, while a large, blurred ring in PDLLA-CHL films.

Table 2 summarizes the typical values of pores size and pores aspect ratio (diameter/depth) when PDLLA was dissolved either in CHL (top) or EA (bottom).

Experimental data clearly demonstrate that pore size is affected by both solvent type and processing conditions, suggesting that the final structure of BF films is determined by both thermodynamic and kinetic contributions.

### 3.3. Contribution of interfacial interactions

In order to relate the structure of porous films to physical and chemical interactions occurring at the interface polymer/solvent/water, we referred to the work by Bolognesi et al. [16]: they linked the relative pore penetration $z_0$ in BF films obtained in a humid flow system to interfacial interactions, namely water surface tension $\gamma_w$, solvent surface tension $\gamma_s$, and water/solvent interfacial tension $\gamma_{w/s}$, as follows (Eq. (1)):

$$z_0 = (\gamma_w - \gamma_{w/s})/\gamma_s \quad (1)$$

according to this model, water drops penetrated the solution and produced multilayer for $z_0$ higher than 1, while for $z_0$ between −1 and 1 the drops float at the interface air/solution, resulting in pore monolayer.

Assuming $\gamma_w = 72.8$ mN m$^{-1}$, $\gamma_{w/s} = 28.3$ mN m$^{-1}$, $\gamma_s = 27.5$ mN m$^{-1}$ for CHL and $\gamma_{w/s} = 25.9$ mN m$^{-1}$, $\gamma_s = 23.9$ mN m$^{-1}$ for EA (Table 1), the relative penetration was calculated as $z_0 = 1.6$ for PDLLA-CHL and $z_0 = 1.9$ for PDLLA-EA. Since these values are higher than 1, the penetration of water drops into PDLLA solutions is thermodynamically favorite either for CHL or EA, with deeper penetration allowed for EA.

The predictions of the model have been compared to the experimental data in Table 2, especially for films produced according to similar processing conditions (i.e., humid flow chamber); the term of comparison was the reciprocal of $z_0$, $1/z_0$, which can be associated to the experimental $R$ value, the pore aspect ratio. When polymer solution of concentration 6% w/v were subjected to controlled humid flow, a good match was observed: PDLLA-CHL produced multilayer

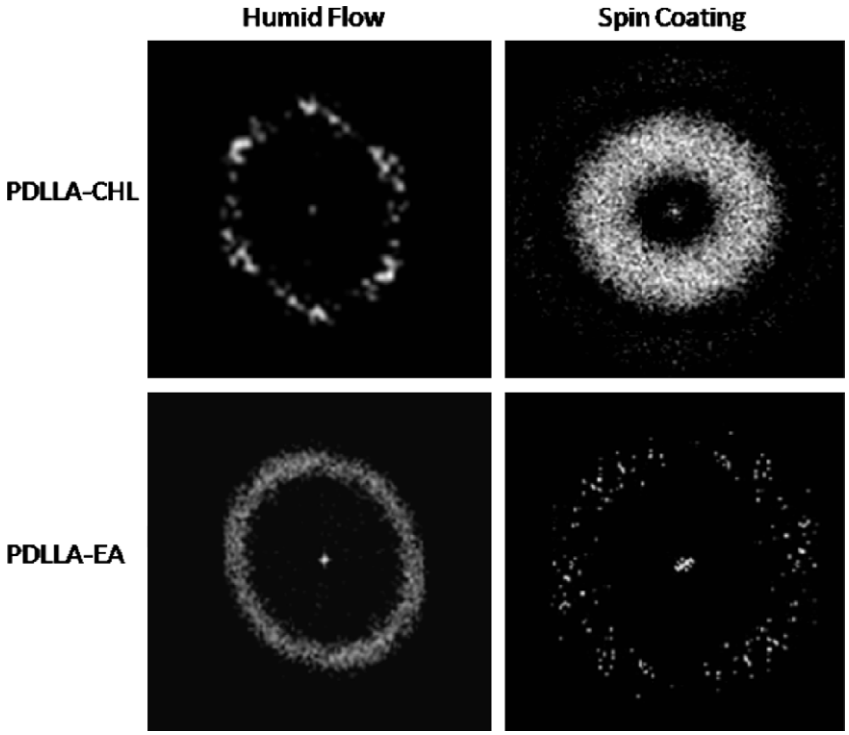


**Fig. 3.** 2D-FFT characterization of surface patterns of BF films. Power spectra show the effects of processing conditions (columns) and solvent type (rows) on the regularity of pore patterns and pore monodispersity.

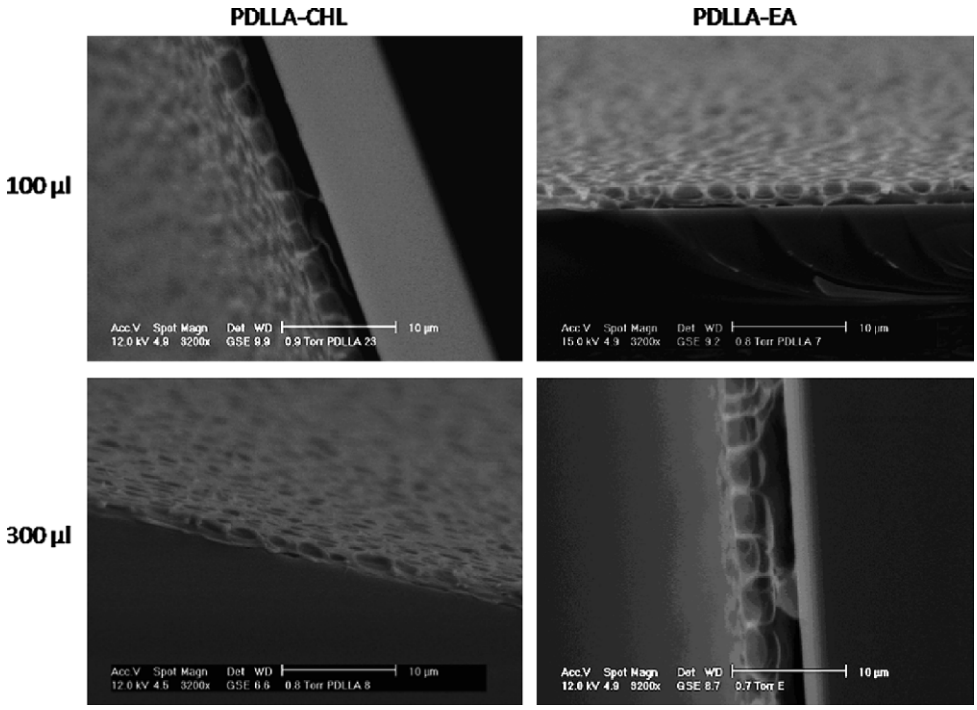


**Fig. 4.** Cross sections of BF films produced via spin coating. The effects of solvent type (columns) and volume of solution (rows) have been evaluated by SEM analysis.

structures as a result of the penetration of water drops and their arrangement in multilayer and $1/z_0 = 1/1.6 = 0.6$ was compatible to the experimental value $R = 0.8$; for PDLLA-EA films the theoretical value $1/z_0 = 1/1.9 = 0.5$ fully corresponded to the experimental $R$ value but multilayer was not obtained, while columnar pores were observed instead. Nevertheless, PDLLA-EA created multilayer when 300 µl of solution were spin coated under controlled humidity. Columnar pores could be related to the higher solubility of water in EA with respect to CHL, that can produce coagulation; alternatively, pore depth can be explained via the low vapour pressure of EA, since during solvent evaporation $\gamma_{w/s}$ decreases and longer time is left to water droplets to continuously penetrate the polymer solution [16].

### 3.4. Contribution of kinetic factors

Despite the good match observed with Bolognesi model, our experimental data suggest that interfacial interactions alone cannot explain the complexity of BF templating, especially when different porous structures have been obtained from the same polymer/solvent system by varying concentration and processing conditions.

Since comparable pore size can be obtained with the same processing system regardless of the type of solvent used, we have hypothesized that kinetics of film drying has an active role in determining BF templating.

In order to support this hypothesis and better clarify the dynamics of the process, it has been recorded in the humid flow system in real time via a microscope camera, as detailed in the Experimental part.

The videos demonstrated that BF templating follows different dynamics depending on the solvent used: in PDLLA-CHL coalescence took place over the entire time domain, even if increasing in the apparent diameter of water droplets was observed just in the last stages of the process and was not detected in the first ones (Fig. 5). Conversely, in PDLLA-EA single droplet growth dominated the first events of BF formation while a burst of coalescence was observed when film hardening became visible.

These findings suggest that in PDLLA-CHL system water drops can be surrounded and eventually covered by a polymer layer, thus allowing (i) in the first stages of the process (diluted solution) the formation of new water droplets and (ii) in the last stages, when the increased concentration of polymer reduces the molecular mobility of the system, the redistribution of existing drops on the top surface and the subsequent increase in pore diameter due to coalescence. This mechanism can account for the formation of multilayers observed in Fig. 2, where pore size increases from the bottom to the top surface.

According to the literature [7], experimental data points have been fitted by $R \sim t^{\alpha}$, resulting in $\alpha = 0.49 \pm 0.02$ for PDLLA-CHL and $\alpha = 0.33 \pm 0.02$ for PDLLA-EA (Fig. 6); these $\alpha$ values reflect the dynamics of droplet growth observed in the videos and confirm the findings of Lymaye et al. [6], where $\alpha \sim 0.3$ is related to single droplet growth and $\alpha \sim 0.5$ to coalescence-dominated growth.

Despite the good agreement of asymptotic fit with the literature, the experimental data in Fig. 6 were best fitted by a Boltzmann sigmoid (Eq. (2)):

**Table 2**
Effects of processing conditions and solvent type on BF films obtained from PDLLA-CHL (top) and PDLLA-EA (bottom) solutions at 6% w/v.

| PDLLA-CHL | Pores Depth (µm) | Pores Diameter (µm) | Pores Aspect Ratio, R |
|---|---|---|---|
| Humid flow ($F = 0.8$ L min$^{-1}$) | 12.9 ± 2.7 | 10.4 ± 0.4 | 0.8 (±21%) |
| Spin coating – 300 µl | 1.7 ± 0.2 | 2.2 ± 0.4 | 1.3 (±18%) |
| Spin coating – 100 µl | 1.0 ± 0.1 | 2.0 ± 0.3 | 2.0 (±15%) |
| **PDLLA-EA** | **Pores Depth (µm)** | **Pores Diameter (µm)** | **Pores Aspect Ratio, R** |
| Humid flow ($F = 1.2$ L min$^{-1}$) | 15.7 ± 0.8 | 7.2 ± 1.6 | 0.5 (±22%) |
| Spin coating – 300 µl | 2.7 ± 0.1 | 3.7 ± 0.8 | 1.4 (±22%) |
| Spin coating – 100 µl | 1.1 ± 0.2 | 1.5 ± 0.1 top<br>1.2 ± 0.1 bottom | 1.4 (±18%)<br>1.1 (±18%) |

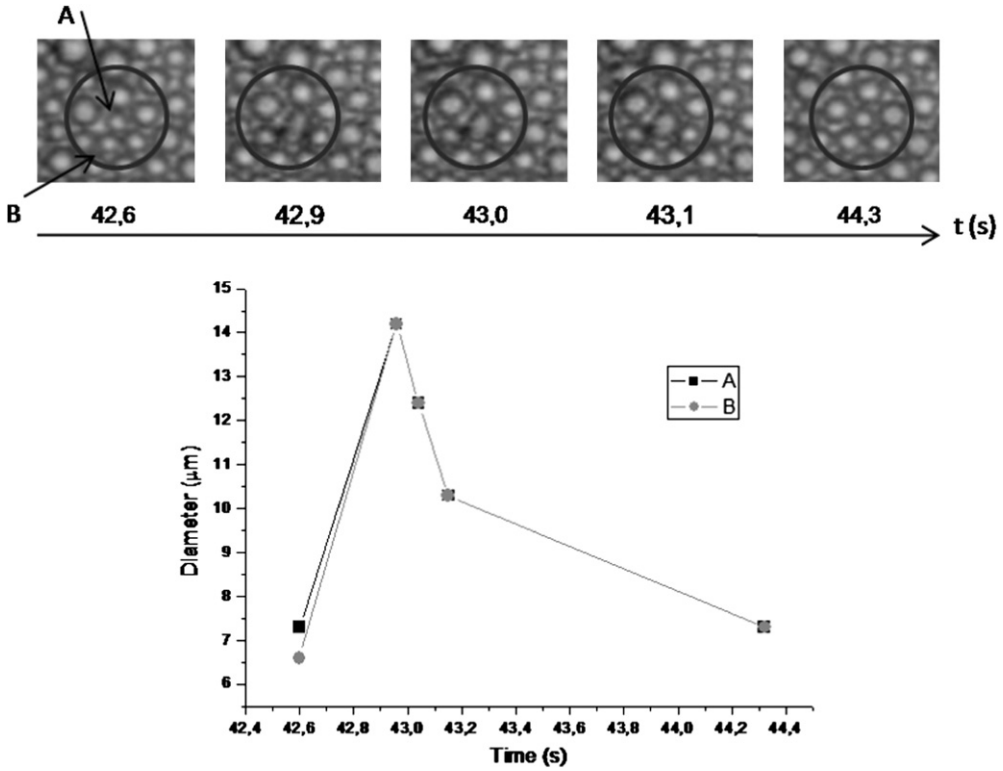


**Fig. 5.** Diameter of drop A and B before, during and after coalescence in the first stages of BF templating in PDLLA-CHL solution.

$$R = \frac{R_f}{1 + e^{-\frac{(t-t_0)}{k}}} \tag{2}$$

where $R_f$ is the final average radius of water drops,

$t_0$ is by definition the time at which $R = R_f/2$

$k$ is related to the slope m of the linear part of the curve by

$$m = \frac{R_f}{4k} \tag{3}$$

the starting radius $R_0$ have been imposed $R_0 = 0$.

Fitting parameters for PDLLA-CHL and PDLLA-EA are reported in Table 3.

The sigmoid fit is in agreement with the cooperative nature of droplet growth by coalescence, clearly shown in the PDLLA-EA video; moreover a kinetic interpretation of $t_0$ and $k$ can be provided if the time evolution of BF patterning is coupled to the kinetics of the evaporation flux approximated to a sigmoid curve. This approximation is justified by the two successive regimes characterizing the drying kinetics of polymer/solvent solutions: in the first stage (diluted solution) the process is fast and mainly controlled by solvent evaporation in air (i.e., heat and mass transfers between the moving interface and the air). In the second stage, as the solvent concentration is decreasing in the upper layer near the interface, the reduction of the partial pressure vapour produces slow diffusion and evaporation [24].

*3.4.1. By expressing the time evolution of the evaporation flux J according to Eq. (4)*

$$J = \frac{1 + e^{-\frac{(t-1-t_0)}{k}}}{1 + e^{-\frac{(t-t_0)}{k}}} - 1 \tag{4}$$

and considering that

$$J_{t_0} = \frac{Js}{2} = \frac{1 + e^{-\frac{(t_0-1-t_0)}{k}}}{1 + e^{-\frac{(t_0-t_0)}{k}}} - 1 = e^{\left(\frac{1}{k}\right)} - 1 \tag{5}$$

where $Js$ is the value of evaporation flux at the starting time of water drop nucleation, which is mainly determined by the solvent vapour pressure and the flux of humid air.

The parameter k can now be written as

$$k = \frac{1}{\ln(Js + 1)} \tag{6}$$

thus demonstrating a relationship between the slope of the curve representing the time evolution of droplet growth and the evaporation flux produced on the polymer solution during the initial stages of BF templating.

This interpretation accounts for the experimental observation that starting from the same polymer-solvent solution larger pores can be produced by decreasing the rate of the humid flux.

The physical meaning of $t_0$ is related to the transition from the fast, evaporation-limited stage of the drying kinetics to the slow, diffusion limited one [26]; $t_0$ can be determined by both polymer concentration and evaporation flux. The videos clearly showed that at $t_0$ PDLLA-EA experienced a burst of coalescence, while in PDLLA-CHL the apparent diameter of water droplets started to increase. Both the phenomena can be related to the reduced mobility of the system caused by the strong solvent/polymer interactions produced in concentrated solutions [27].

Starting from our experimental observations the following model for BF templating is hereby proposed (Fig. 7): upon the exposure of evaporating polymer solution to a flow of humid air, the cooling of polymer surface favors the condensation of water vapour and water droplets undergo a burst of nucleation at the interface; the flow can be directly introduced in a chamber or indirectly produced upon spin coating the polymer solution in environments with high values of

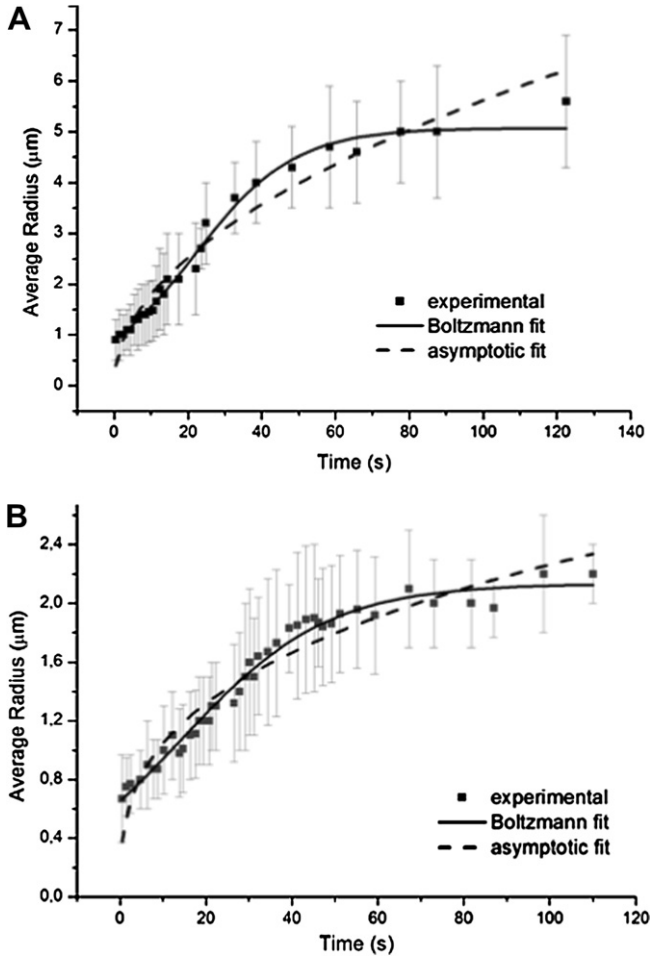


**Fig. 6.** Data fitting of experimental data points reporting the average radius of water droplets as a function of drying time in PDLLA-CHL (A) and PDLLA-EA (B).

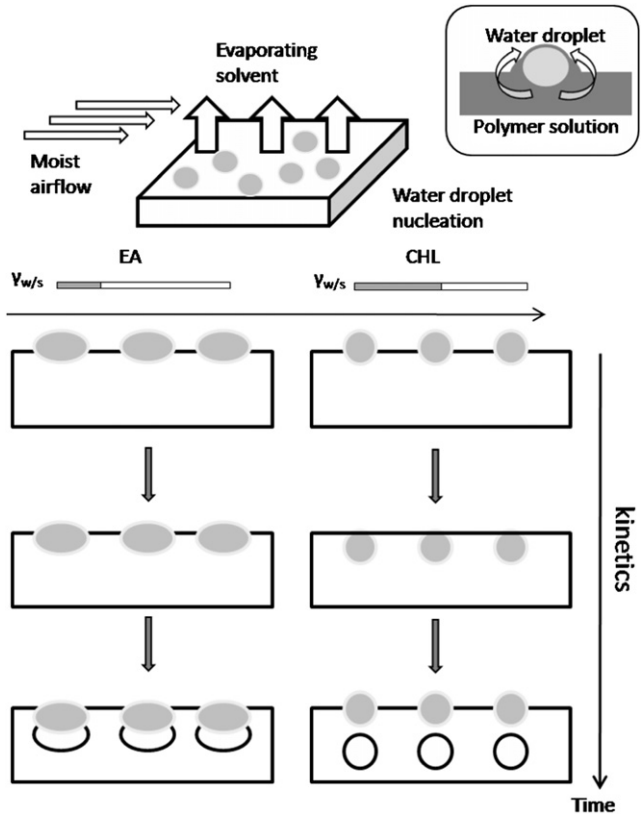


**Fig. 7.** Mechanism proposed for Breath Figure templating on PDLLA-EA, and PDLLA-CHL. The interplay of kinetics of film hardening and water-solvent interfacial interactions determines the structure of BF films.

relative humidity. According to specific water/solvent interfacial interactions water drops start to grow via diffusion limited (e.g., PDLLA-EA) or coalescence-driven growth (e.g., PDLLA-CHL), thus producing a population of monodisperse drops. If proper interfacial conditions are satisfied, the polymer solution can surround them all around until film hardening occurs (Fig. 7). When solvents with proper interfacial properties are subjected to slow evaporation (represented by high $t_0$ and k values in the Boltzmann sigmoid), a new layer of polymer solution is produced at the interface with air; new water drops can nucleate and grow via coalescence, resulting in BF films with pore multilayers. Conversely, just a monolayer is observed for fast film hardening despite favorable water/solvent interfacial tension, as appears by comparing PDLLA-CHL films produced in the humid flow chamber with the ones obtained via spin coating.

These findings exclude that solvent density has a key role in the determination of pore monolayer/multilayer, as proposed by earlier works: controversial opinions have been advanced, with some authors reporting the formation of monolayer from solvents denser than water [2,19], while other papers showed opposite results [12]. Two main considerations have suggested the non influential role of solvent density: (i) interfacial forces overcome gravitational forces for water drops whose size is compatible with pores observed in our BF films and (ii) either pore monolayer or multilayers have been produced by the same polymer solution (e.g., PDLLA-EA), just acting on the processing conditions.

**Table 3**
Fitting parameters for PDLLA-CHL and PDLLA-EA obtained by Boltzmann sigmoid fit.

| Solvent | $R_f$ | $t_0$ | $k$ | Reduced chi$^2$ |
|---|---|---|---|---|
| CHL | 5.14 ± 0.09 | 21.8 ± 0.9 | 14.2 ± 0.8 | 0.03 |
| EA | 2.14 ± 0.03 | 14.1 ± 0.7 | 17.2 ± 0.8 | 0.004 |

## 4. Conclusions

Porous PDLLA substrates with a variety of structures were obtained via Breath Figure templating, by varying the physical and chemical properties of polymer solution and processing conditions; this approach was pursued to evaluate the contribution of interfacial interactions and kinetic factors to BF phenomenon. Starting from phenomenological observations, our study has indicated that the entire process is governed by the interplay of kinetic factors and interfacial interactions (Fig. 7). In particular, interfacial tension between the evaporating solvent and condensing water mainly accounts for pore diameter and regulates the ability of polymer solution to surround water droplets, leading to pore multilayer films for suitable drying time. On the other side the rate of film hardening can define the actual structure of BF films: our modellization based on Boltzmann sigmoid could explain the time evolution of pore size in terms of solvent vapour pressure, humid flow rate, and polymer concentration. Moreover, the kinetics of film drying overcomes the contribution of interfacial interactions, hindering the formation of pore multilayers despite thermodynamics allows the process. The careful evaluation of the kinetics of film hardening and interfacial forces developed between evaporating polymer solution and condensing water represent a powerful tool for tuning the structure and pore size of BF films, making them suitable for several applications.

## Acknowledgements

The authors thank Mr. Lorenzo Moschini for SEM analysis.

This work has been partially funded by the Italian Ministry of University and Research.

## References

[1] Bunz UHF. Adv Mater 2006;18:973–89.
[2] Widawski G, Rawiso M, François B. Nature 1994;369:387–9.
[3] Rayleight Lord. Nature 1911;86:416–7.
[4] Beysens D, Knobler CM. Phys Rev Lett 1986;57:1433–6.
[5] Briscoe BJ, Galvin KP. J Phys D 1990;23:422–8.
[6] Limaye AV, Narhe RD, Dhote AM, Ogale SB. Phys Rev Lett 1996;76:3762–5.
[7] Pitois O, Francois B. Colloid Polym Sci 1999;277:574–8.
[8] Peng J, Han Y, Yang Y, Li B. Polymer 2004;45:447–52.
[9] Zhao B, Li C, Lu Y, Wang X, Liu Z, Zhang J. Polymer 2005;46:9508–13.
[10] Stenzel MH, Barner-Kowollik C, Davis TP. J Polym Sci Part A Polym Chem 2006;44:2363–75.
[11] Chan DYC, Henry JD, White LR. J Colloid Interface Sci 1981;79:410–8.
[12] Srinivasarao M, Collings D, Philips A, Patel S. Science 2001;292:79–83.
[13] Dell'Aversana P, Banavar JR, Koplik J. Phys Fluids 1996;8:15–28.
[14] Dell'Aversana P, Tontodonato V, Carotenuto L. Phys Fluids 1997;9:2475–85.
[15] Karthaus O, Maruyama N, Cieren X, Shimomura M, Hasegawa H, Hashimoto T. Langmuir 2000;16:6071–6.
[16] Bolognesi A, Mercogliano C, Yunus S, Civardi M, Comoretto D, Turturro A. Langmuir 2005;21:3480–5.
[17] Park MS, Joo W, Kim JK. Langmuir 2006;22:4594–8.
[18] Pitois O, Francois B. Eur Phys J B 1999;8:225–31.
[19] Jenekhe SA, Chen XL. Science 1999;283:372–5.
[20] Nishikawa T, Nonomura M, Arai K, Hayashi J, Sawadaishi T, Nishiura Y, et al. Langmuir 2003;19:6193–201.
[21] Zhao B, Zhang J, Wang X, Li C. J Mater Chem 2006;16:509–16.
[22] Chaudhuri JB, Davidson MG, Ellis MJ, Jones MD, Wu XJ. Macromol Symp 2008;272:52–7.
[23] Steyer A, Guenoun P, Beysens D, Knobler CM. Phys Rev B 1990;42:1086–9.
[24] Guerrier B, Bouchard C, Allain C, Benard C. AIChE J 1998;44:791–8.
[25] Zielinski JM, Duda JL. AIChE J 1992;38:405–15.
[26] Lide DR. Handbook of chemistry and physics. 82nd ed. CRC; 2001.
[27] Yaws CL. In: Yaws CL, Andrew W, editors. Thermophysical properties of chemicals and hydrocarbons; 2008. Norwich, NY.